PAPER

Thermal sublimation: a scalable and controllable thinning method for the fabrication of few-layer black phosphorus

To cite this article: Weijun Luo *et al* 2017 *Nanotechnology* **28** 285301

View the article online for updates and enhancements.

Related content

- Enhanced dielectric deposition on single-layer MoS2 with low damage using remote N2 plasma treatment
Qingkai Qian, Zhaofu Zhang, Mengyuan Hua et al.
- In situ observation of the thermal stability of black phosphorus
Shenghuang Lin, Yanyong Li, Wei Lu et al.
- Mechanical exfoliation and layer number identification of MoS2 revisited
L Ottaviano, S Palleschi, F Perrozzi et al.

Recent citations

- Applications of Phosphorene and Black Phosphorus in Energy Conversion and Storage Devices
Jinbo Pang *et al*

IOP ebooks™

Bringing you innovative digital publishing with leading voices to create your essential collection of books in STEM research.

Start exploring the collection - download the first chapter of every title for free.

This content was downloaded from IP address 130.126.162.126 on 06/07/2018 at 22:20

Nanotechnology **28** (2017) 285301 (12pp) https://doi.org/10.1088/1361-6528/aa76ae

Thermal sublimation: a scalable and controllable thinning method for the fabrication of few-layer black phosphorus

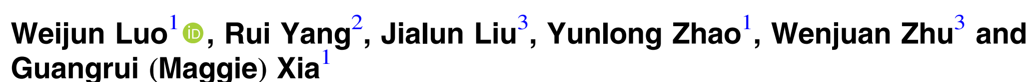

Weijun Luo[1], Rui Yang[2], Jialun Liu[3], Yunlong Zhao[1], Wenjuan Zhu[3] and Guangrui (Maggie) Xia[1]

[1] The University of British Columbia, Department of Materials Engineering, Vancouver, B.C., V6T1Z4, Canada
[2] The University of British Columbia, Department of Physics and Astronomy, Vancouver, B.C., V6T1Z4, Canada
[3] The University of Illinois at Urbana-Champaign, Department of Electrical and Computer Engineering, Champaign, IL 61801, United States of America

E-mail: gxia@mail.ubc.ca

Received 22 February 2017, revised 31 May 2017
Accepted for publication 2 June 2017
Published 20 June 2017

Abstract

We report uniform layer-by-layer sublimation of black phosphorus under heating below 600 K. The uniformity and crystallinity of BP samples after thermal thinning were confirmed by Raman spectra and Raman mapping. The sublimation rate of BP was around 0.18 nm min^{-1} at 500 K and 1.15 nm min^{-1} at 550 K. Both room and high temperature Raman peak intensity ratio $\frac{\text{Si}}{\text{A}_g^2}$ as functions of BP thickness were established for *in situ* thickness determination and control. Uniform and crystalline 2 to 4-layer BP flakes with areas from 10 to 1000 μm^2 were prepared with this method. No micron scale defects were observed. The sublimation thinning method was shown to be a controllable and scalable approach to prepare high-quality few-layer black phosphorus.

Supplementary material for this article is available online

Keywords: Raman spectroscopy, black phosphorus, thermal thinning

(Some figures may appear in colour only in the online journal)

1. Introduction

Semiconducting orthorhombic black phosphorus (BP), like graphene, is a layer-stacked 2-dimensional (2D) nanomaterial with sp^3-hybridized phosphorus atoms covalently bonded to a puckered structure via weak van der Waals forces [1]. The energy band gap, close to 2 eV, has been measured by scanning tunneling spectroscopy from monolayer BP [2]. With the increasing number of layers, the band gap decreases, and finally reaches 0.3 eV for bulk BP [3]. This tunable band gap enables BP to be a promising candidate for applications in field effect transistors [4–8]. Other efforts have shown its prospective applications in gas sensors [9], lithium-ion batteries [10], thermoelectric devices [11, 12], and photo-transistors [13, 14].

So far, there remain two major challenges for BP research: the air-stabilization and the controllable fabrication of ultra-thin BP layers [15]. To address the former problem, the passivation of BP was successfully achieved via chemical modification method like covalent aryl diazonium functionalization [16] and physical encapsulation methods such as atomic layer deposited dielectric passivation [17] or h-BN passivation [18]. However, current top-down methods in preparing ultra-thin BP such as mechanical exfoliation [19], anodic oxidation and water rinsing [20], shear exfoliation [21–23] in liquids, and plasma thinning [24–26] still could not be used for scalable and controllable production of large uniform few-layer BP. Moreover, poor uniformity, scalability and crystallinity of BP thin films prepared by bottom-up

 © 2017 IOP Publishing Ltd Printed in the UK

methods such as pulsed laser deposition [27, 28] and chemical vapor deposition (CVD) [27] remained as critical obstacles for industry application. Hence, the development of a scalable and controllable method to fabricate few-layer BP with good uniformity and crystallinity is critical for BP applications.

According to our best knowledge, thermal thinning has been used as a top-down thinning method in preparing few-layer 2D materials. Huang *et al* [29] showed successful preparation of large (>10 μm^2) and thin (1–2 nm) 2D Bi_2Se_3 and Sb_2Te_3 crystals by sublimation thinning. Lu *et al* [30] reported thermal thinning of tungsten telluride (WTe_2) flake with its original lattice structure.

In addition, two studies on the mechanism of thermal thinning of BP were reported: in 2015, Liu *et al* [31] first observed the sublimation of BP at 400 °C starting from the formation of eye-shaped cracks along $\langle 001 \rangle$ directions by *in situ* transmission electron microscopy. After that, in 2016, another work [32] further indicated the sublimation of BP took place at 375 °C and the process involved detachments of pairs of P atoms.

Furthermore, Raman spectroscopy can serve as a fast and non-destructive method to identify the thickness (the layer number *N*) of 2D material flakes [33]. For instance, Li [34] determined the number of graphene layers up to 100 layers according to the Raman peak intensity ratio of $\frac{I(\mathrm{G})}{I(\mathrm{Si})}$; similarly, the layer number of MoS_2 can also be determined by $\frac{I(\mathrm{E}^1_{2g})}{I(\mathrm{Si})}$ and $\frac{I(\mathrm{A}_{1g})}{I(\mathrm{Si})}$. So far, for BP, $\frac{I_{\mathrm{A}^1_g}}{I_{\mathrm{Si}}}$ [19] and $\frac{I_{\mathrm{Si}}}{I_{\mathrm{A}^2_g}}$ [24] as functions of layer numbers *N* have been reported. Therefore, with a specific excitation wavelength, the layer-number-dependent Si Raman intensity from underlying SiO_2/Si substrates can be used as a probe for on-site thickness monitoring. In this work, we investigated of the relationship between the thickness (the layer number *N*) and the Raman intensity ratio $\frac{I_{\mathrm{Si}}}{I_{\mathrm{A}^2_g}}$.

The work was organized with the following order: first of all, we reported on the layer-by-layer uniform sublimation of bulk BP flakes (~100 nm) in the temperature range from 500 K (227 °C) to 600 K (327 °C) in high purity nitrogen gas ambient; next, we investigated the thinning rates of BP at 500 K and 550 K, respectively; then we recorded Raman peak intensity ratios $\frac{I_{\mathrm{Si}}}{I_{\mathrm{A}^2_g}}$ of the A^2_g mode of BP and the underlying Si (100) acquired at both high temperatures (500 and 550 K) and room temperature as functions of BP thickness, which can be used as an *in situ* BP thickness indication for controlled thinning; after that, we successfully and repeatedly prepared 3 independent few-layer (less than 4 layers) crystalline BP flakes with areas all over 200 μm^2; at last, we demonstrated the successful thermal thinning of BP on graphene/Si substrate.

2. Methods

2.1. Thermal sublimation

The BP flakes were mechanically exfoliated (4–5 times at most) from bulk BP crystals (99.998%, Smart Elements, Vienna, Austria) in a glove box using Nitto SPV 224 R tape and then transferred directlty to a pre-cleaned Si (100) wafer (4 inch, 0.56 mm thick, with a 300 nm thick thermal-grown SiO_2 layer). On the other hand, in order to prepare large and flat BP flakes on graphene substrate, the exfoliated BP on the tape was transferred to a Gel-Pak^{TM} sticky gel-box, and a CVD multiple-layer graphene/Si wafer substrate (prepared following the previous report [35]), was pressed tightly onto the gel-box to transfer BP flakes onto the graphene/wafer substrate. Then, the wafers were cut into small pieces (4 mm × 4 mm). After that, a wafer piece with large and flat BP samples was selected and loaded into an enclosed Linkam TS1200 heating stage one at a time with high purity nitrogen gas (Praxair, industrial grade, purity: 99.995%) purging into the chamber before heating. The heating stage was then mounted on the motorized *XY* stage of a Horiba Scientific LabRAM HR800 con-focal Raman microscope. After that, an isothermal joule heating process was performed with one small piece of wafer placed on a sapphire plate in the chamber of the heating stage with nitrogen gas flowing through the chamber. The ramping-up and cooling-down rates were 100 K min^{-1}.

2.2. Raman measurement

In section 3.2, all Raman measurements were performed with a Horiba LabRam HR800 Raman system in the back-scattering configuration with the excitation wavelength of 441.6 nm. The Raman spectra were collected through an Olympus 50X (NA = 0.55) objective lens and recorded with the grating of 2400 lines mm^{-1} which has a spectral resolution of 0.27 cm^{-1}. When performing Raman measurement at 500 K/550 K, we reduced the laser power to be less than 0.2 mW μm^{-2} by adding a filter in order to minimize the heating effect induced by the laser power. The acquisition time and accumulation times were optimized with 6 s and 2 times, respectively, in order to get a signal-to-noise ratio of 100 approximately as well as avoid long time laser damage to BP samples. Furthermore, in this section, all 2D Raman mapping images were acquired using the following configurations: the increments of *X* and *Y* direction were 1.6 and 1.5 μm per step, respectively. The laser spot size was ~2 μm^2. In addition, during Raman mapping measurements, all BP flakes were placed in the heating stage and purging with high purity nitrogen gas in order to avoid oxidation.

In section 3.3, all Raman measurements were performed with a Horiba LabRam HR800 Raman system in the back-scattering configuration with the excitation wavelength of 632.8 nm. The Raman spectra were collected through an Olympus 50X (NA = 0.55) objective lens and recorded with the grating of 600 lines mm^{-1} which has a spectral resolution of 0.63 cm^{-1}. The acquisition time and accumulation times were optimized with 3 s and 2 times, respectively. Moreover, in this section, all 2D Raman mapping images were acquired using the following configurations: the increments of *X* and *Y* direction were 1.2 and 1.1 μm per step, respectively.

2.3. Determination of crystallographic orientations (CO) of BP and underlying Si (100) substrate

In the same manner as previous studies [36–38], the incident laser beam was polarized, and an analyzer was placed in the parallel configuration before the Raman signals enter the spectrometer. BP samples were placed on a rotation stage and rotated 180° about the microscope optical axis in 12 steps (15°/step). Considering the periodicity of A_g^1 and A_g^2 modes are 180° and the maximum Raman intensity of A_g^1 and A_g^2 modes are orthogonal [38, 39], the maximum Raman intensity of A_g^1 or A_g^2 mode could be easily measured with rotating only 90° (6 steps). In this work, samples were oriented to maximize the Raman intensity of the A_g^1 mode. What's more, since the rotation angle acquired from the previous 6-step operation might be still rough from the real angle with the maximum Raman intensity of A_g^1 mode, the half-interval search method was used for further refinement to get a more precise angle. Similar procedures were performed at the underlying Si (100) substrates to find the maximum and minimum Si Raman intensity. In addition, during every step, the laser spot was focused at the same point on the sample to ensure the consistency of results.

2.4. Atomic force microscopy (AFM)

AFM measurements were performed using the contact mode with an Asylum Research Molecular Force Probe 3D AFM and a Bruker AFM System. Before transferring to AFM measurements, samples were stored in a glove box filled with high purity argon gas and the concentrations of O_2 and H_2O in the glove box were less than 0.2 ppm, to minimize the oxidation of BP while performing the AFM measurements in the air ambient.

3. Results and discussion

3.1. Uniform color changes with no observable cracks during the isothermal Joule heating

Here, we reported uniform color changes with no observable changes of area during the isothermal joule heating under the protection of high purity nitrogen gas, instead of any shrinkage of area. In figure 1(A), it illustrates the sublimation process, and figures 1(B)–(F) show the optical images of a BP sample on the SiO_2/Si substrate at four different times during 600 K heating from 0 to 51 min.

The sample colors, which are directly related to the thickness, obviously changed. In figure 1(B), the pink zone (labeled as 'Area 2') was thinner than the green zone ('Area 1'). Figure 1(C) shows 'Area 1' turned to white and 'Area 2' to light green after heating for 11 min. Figure 1(D) shows 'Area 1' turned to red and 'Area 2' to peach after heating for 21 min. In figure 1(E), 'Area 2' turned to gray at 41 min, which was in consistent with the characteristic color of few-layer BP in previous work [19, 24]. At 51 min, figure 1(F) shows 'Area 2' is fully disappeared. The thickness-dependence of BP flake colors could be attributed to the light interference effect for BP flakes of different thicknesses. During the full process, the area of the sample remained and the colors of each region uniformly changed, which suggested that the sublimation process was uniform and happened layer-by-layer.

In addition, we performed high temperature heating on 2 BP flakes at 500 and 550 K, respectively. 2D Raman mapping and thickness measurements by AFM at the 2 BP flakes were taken before and after high temperature heating. Figures 2(A) and (D) showed the optical images of a 36 nm thick BP flake, which was reduced to 13 nm thick after heating at 500 K. The 2D Raman maps of A_g^1 and A_g^2 modes of the pristine 36 nm thick flake are shown in (B) and (C), and those of the flake after heating for 120 min are shown in (E) and (F). These Raman peak intensities were uniform across the sample, showing that the BP sample kept its integrity and uniformity after the heating process, which confirmed the isotropic layer-by-layer sublimation of BP. This is also supported by another flake heated at 550 K for 25 min shown in figures S1(A)–(F) of the supplementary information available online at stacks.iop.org/NANO/28/285301/mmedia.

In contrary, previous studies [31, 32, 40] all reported the sublimation and decomposition of BP were above 350 °C (623 K). Though the oxidation of BP caused by trace impurities such as water and oxygen in nitrogen gas during heating might take place, we attributed the self-separation of BP was the main reason for the sublimation instead of oxidation-sublimation. The oxidation conditions have been widely studied before: Favron *et al* [41] first indicated that light, oxygen and water were three factors cause the oxidation of BP; Luo *et al* [18] reported that with 5% oxygen/Ar or 2.3% H_2O/Ar, the oxidation rate is <5 Å for 5 h from XPS results; Wang *et al* [42] reported BP could remain stable in pure water without the presence of oxygen molecules from nuclear magnetic resonance spectroscopy results; Li *et al* [43] reported that heating could remove the metastable oxygen adsorbed on the surface of BP. Therefore, according to those studies on oxidation processes and mechanisms of BP, it could be concluded that with the protection of high purity (99.995%) nitrogen gas, the sublimation of BP in this work could be described as a physical process of layer separation.

3.2. BP thinning rates at 500 and 550 K

After confirming the sublimation method could be used for thinning thick BP flakes, we investigated the thinning rates of BP at 500 and 550 K, respectively. The investigations consist of 4 parts: (1) determination of the CO of BP and underlying Si (100) substrate; (2) and (3) 'interrupted' and 'continuous' thinning on 4 independent BP flakes heated at 500 K and 550 K, respectively; (4) Raman intensity ratios $\frac{I_{Si}}{I_{A_g^2}}$ as a function of the BP thickness (the layer number N).

3.2.1. Determination of the CO by angle-resolved polarized Raman spectroscopy (ARPRS). Before each heating step, it was important to identify the CO of the samples and rotate them to convenient angles relative to the excitation laser polarization

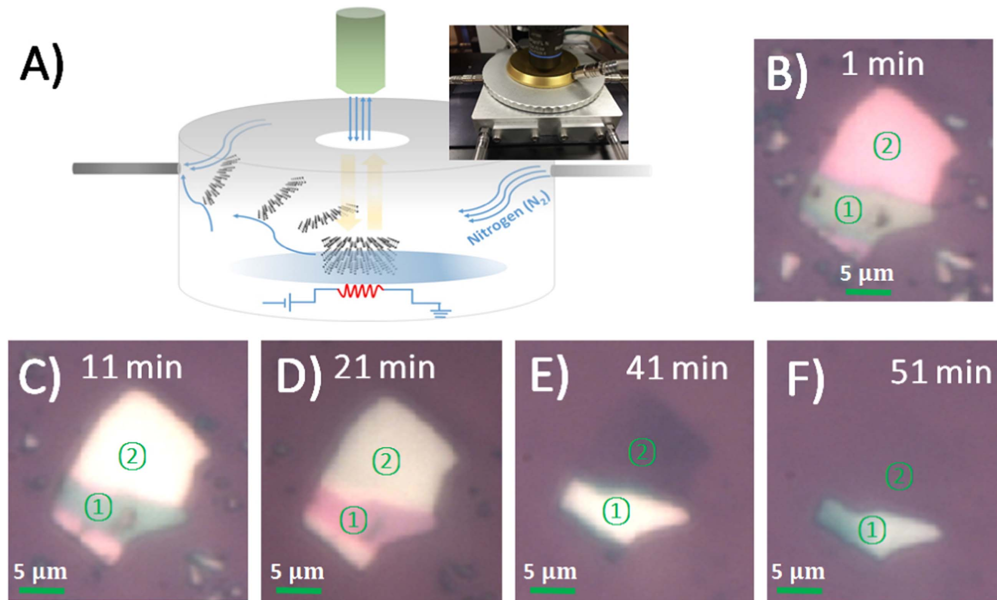

Figure 1. (A) Illustration of the sublimation process of BP and the inset shows the heating stage used; (B)–(F) the optical images of the layer-by-layer sublimation process of BP at 600 K. The different colors in 'Area 1' and 'Area 2' indicate different thickness.

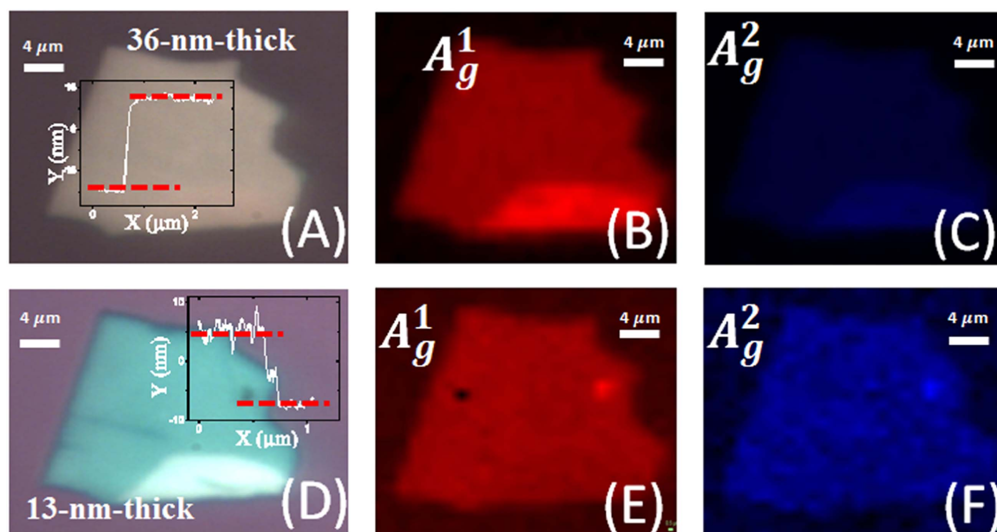

Figure 2. (A) The optical image of a 36 nm thick BP flake before the 500 K thinning process; (B) and (C) the spatial Raman maps of the A_g^1 and A_g^2 peak intensity acquired on this BP flake; (D) the optical image of this BP flake after the 500 K thinning process for 120 min, which was reduced to 13 nm thick; (E) and (F) the Raman images (the A_g^1 and A_g^2 modes) of another 85 nm thick BP flake after the 500 K thinning process.

angle such that the Raman signals can be maximized. There is a strong Raman intensity dependence on the CO of BP and Si. Thus, identifying the CO of BP and Si (100) becomes a prerequisite. According to previous reports [36, 38], A_g^1 and A_g^2 modes of BP have their maximum Raman intensities at orthogonal directions. In this work, we rotated samples A and C to have maximum A_g^1 and minimum A_g^2 Raman intensities and kept their positions unchanged during the heating and Raman measurements. In choosing these samples, we also made sure that the Si Raman intensity was close to the maximum Si peak.

In figure 3(A), a single flake (named 'Sample A', see the inset picture) was rotated to the right angle with the maximum Raman intensities of A_g^1 mode and the minimum Raman intensity of A_g^2 mode. There were 3 areas in 'Sample A' with different colors indicating different thickness. The Raman intensity dependence on the rotation stage angle reading of 'Area 1' was recorded and shown in figure 3(B). When the rotation stage angle was 95°, the A_g^1 model reached its maximum Raman intensity, where A_g^2 peak reached its minimum; while the Si peak signal was reasonably high for Raman measurements. Similarly, in figure S2(A) of supplementary information, another flake (named 'Sample B', see the inset picture) with two areas in different colors was chosen for CO determination by ARPRS in the same manner

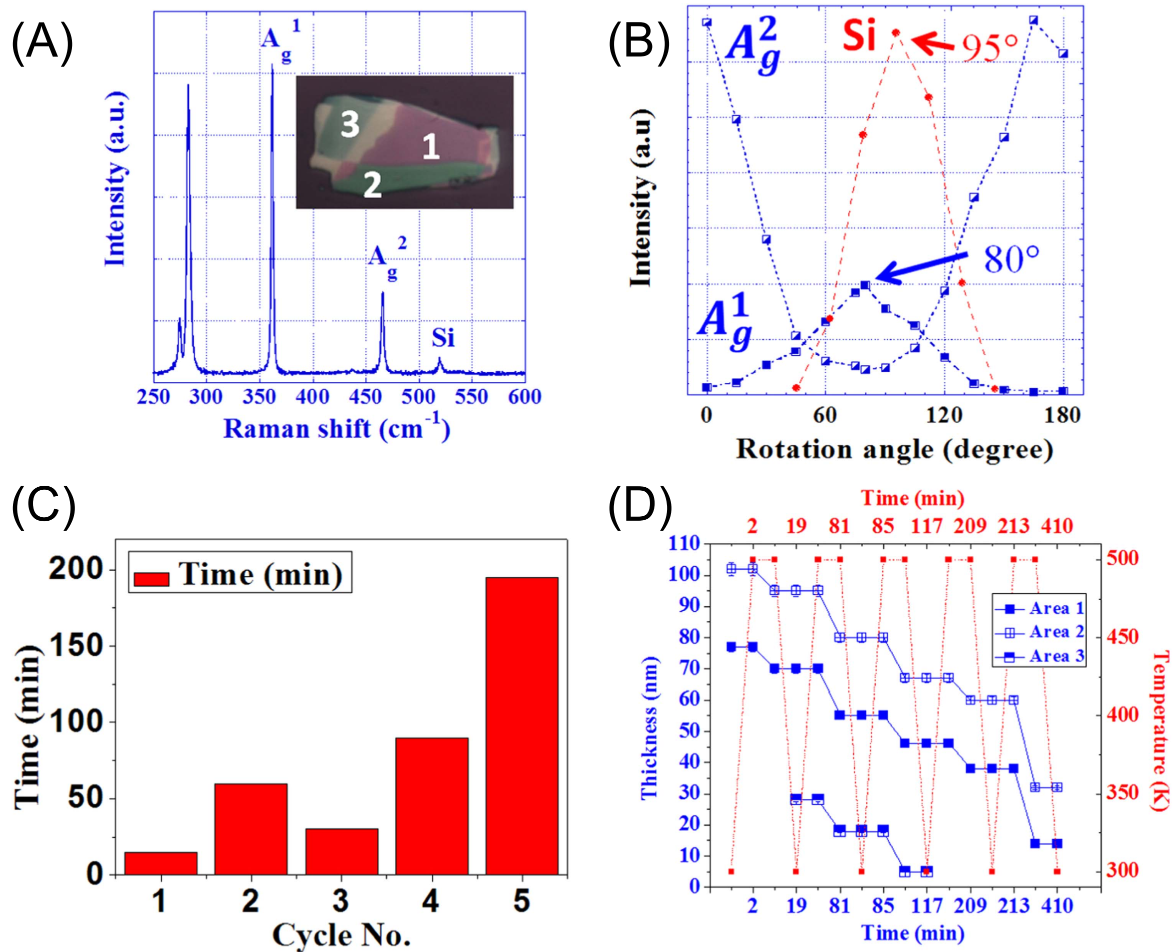

Figure 3. 'Sample A'. (A) The Raman spectrum with maximum intensity of A_g^1 mode and minimum intensity of A_g^2 mode (the inset picture shows 'Sample A' to be heated at 500 K, the numbers indicate different areas of this sample); (B) the Raman intensities of A_g^1 and A_g^2 modes of BP and underlying Si (100) peak as functions of rotation angle; (C) time for each heating cycle of the 'interrupted heating' process performed at 'Sample A'; (D) the measured thickness in different areas of 'Sample A' as a function of time.

like 'Sample A', and the angle-dependent Raman intensity results of BP and Si were shown in figure S2(B) of supplementary information.

What's more, the angle-dependent polarized Raman response of underlying Si (100) is a sinusoidal function which has a periodicity of 90° [44, 45]. In consideration of penetration depth and further investigation in Raman intensity ratios $\frac{\mathrm{Si}}{A_g^2}$ as a function of thickness, we preferred the rotation angle difference between maximum Raman intensity of A_g^1 mode and that of Si (100) should be equal or less than 15°. In other words, when A_g^1 mode of BP is maximized, more than 50% of maximum Raman intensity of the underlying Si (100) can still be measured. In figure 3(B), the intensities of BP A_g^1 and A_g^2 modes as well as underlying Si (100) substrates are plotted as functions of rotation angles. The rotation angles of maximum A_g^1 and Si intensity of 'Sample A' showed a difference of 15°. In figure S2(B), those of 'Sample B' also showed a difference of 15°.

3.2.2. Interrupted and continuous thinning at 500 and 550 K.

After that, we performed more thinning experiments to study the thinning rates. AFM measurements were made to monitor the thickness changes. However, for that purpose, it was necessary to remove the samples from the heating stage, and we termed this type of thinning as 'interrupted thinning'. The 'interrupted heating' was conducted on 'Sample A' at 500 K with 5 cycles of thinning. The heating durations for each heating step are shown in figure 3(C). The thicknesses before and after each thinning step were acquired by AFM measurements, and are shown in figure 3(D). The characteristic colors of different thickness were recorded as well.

In figure 3(D), for each thinning cycle, each area was reduced by the same amount, revealing that different areas underwent isotropic sublimation rates. After that, in figures S2(C) and (D), 'Sample B' with 2 different areas was heated at 550 K for 6 cycles. The heating durations for each heating step are shown in figure S2(C), and the recorded thicknesses plotted in figure S2(D). Clearly, at 550 K, sublimation took place uniformly in different areas.

Moreover, after thinning at 500 K for about 100 min, the thickness of 'Area 3' (see circled area in figure 4(A)), was reduced to ~5 nm, which can be seen in figure 4(B). In figure 4(C), Raman intensities of A_g^1 and A_g^2 remain strong while the Si Raman intensity is increased in comparison with

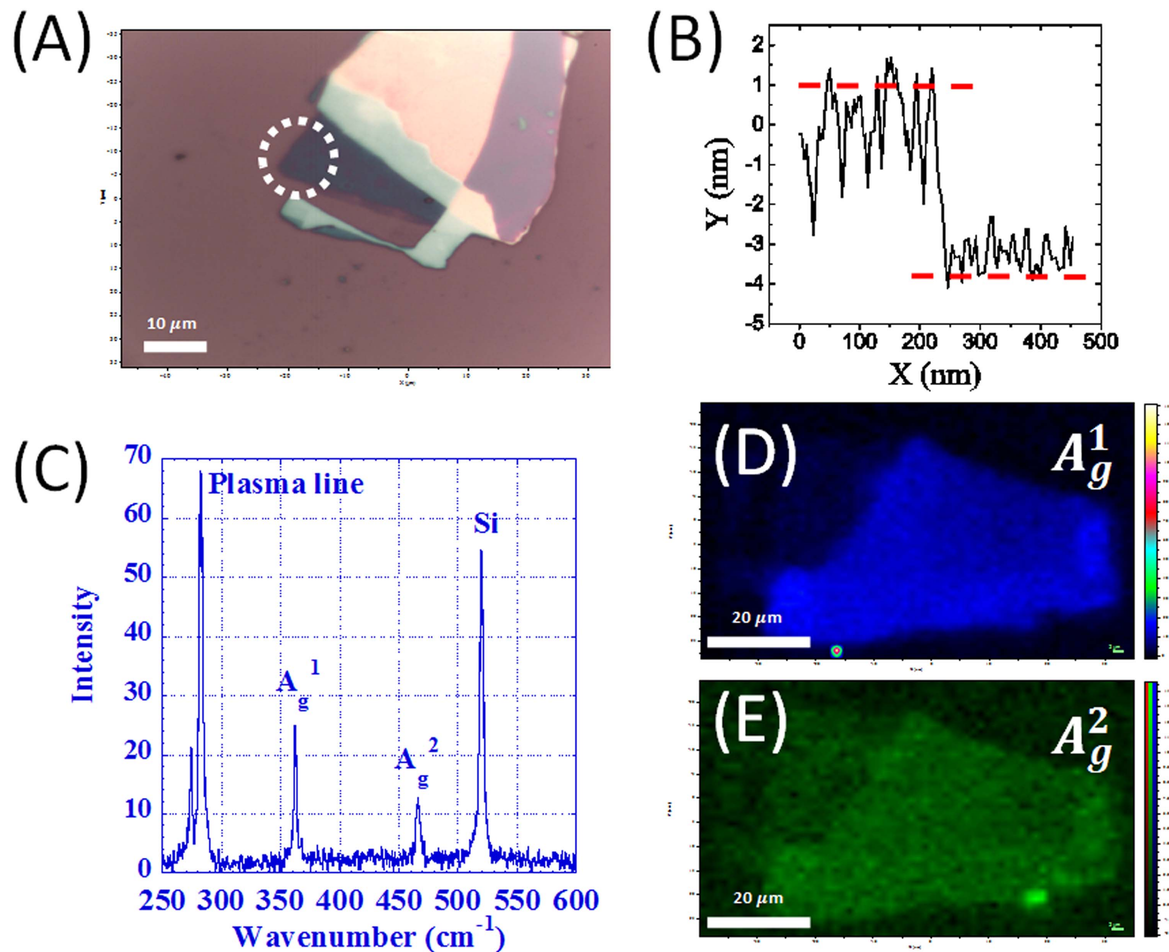

Figure 4. (A) The optical image of 'Area 3' in 'Sample A'; (B) the AFM profile of the circled area in (A); (C) the Raman spectrum collected at circled area in (A); (D) and (E) the spatial Raman maps of the peak intensities of A_g^1 and A_g^2 modes which demonstrate the integrity and crystallinity of 'Area 3'.

the Raman spectrum of the original sample shown in figure 3(A). In figures 4(D) and (E), the spatial Raman maps of A_g^1 and A_g^2 modes indicated the uniformity and crystallinity of 'Area 3'. The area of this 5 nm thick flake is of 180 μm^2. Since the thickness of single-layer BP is about 0.5 nm [46], 'Area 3' was estimated to have 9–10 layers.

To get the accurate thinning rates at different temperatures without the interruptions and the exposure to air during the AFM measurements, continuous thinning processes were performed on 'Sample C' and 'Sample D' at 500 K and 550 K, respectively (the detailed images were included in figures S3 and S4 of supplementary information). The *in situ* Raman spectra were collected during heating, which are shown in figures 5(A) and (B). As BP flakes were thinned down, the Raman intensity ratios of Si (100) over that of the BP peaks increased. We indicated the Raman data would be used as an *in situ* thickness monitor and a thickness control method as discussed below. In figure 5(C), the thickness of 'Sample C' was reduced from 85 to 45 nm after thinning process at 500 K for 221 min. The gradual color changes were recorded (images were included in figure S4 of supplementary information). The thicknesses of each color were read from the color-thickness map (see background of figures 5(C)–(F)) generated previously based on AFM measurements. The estimated thickness as a function of time is shown in figure 5(C). In figure 5(D), the thickness of 'Sample D' was reduced from 105 to 45 nm after thinning process at 550 K for 51 min. Similarly, the thickness-time profile of 'Sample D' heated at 550 K was also plotted in figure 5(D). Also, in figures 5(C) and (D), the thickness-time profiles of the samples with 'interrupted and continuous heating' are compared. There were some slight differences between them, which could be attributed to the air exposure and oxidation of the 'Sample A' and 'Sample B' for 'interrupted heating' might affect the AFM thickness results. For 'interrupted heating', the average thinning rate was $\sim$0.19 nm min^{-1} at 500 K and $\sim$1.02 nm min^{-1} at 550 K, respectively; for continuous thinning, the thinning rates were $\sim$0.18 nm min^{-1} at 500 K and $\sim$1.15 nm min^{-1} at 550 K, respectively, which were in agreement with the 'interrupted heating' results.

3.2.3. Raman peak intensity ratios $\frac{I_{Si}}{I_{A_g^2}}$ as a function of BP thickness. In this work, we investigated the thickness—dependent Raman intensity ratio $\frac{I_{Si}}{I_{A_g^2}}$. As mentioned above, the

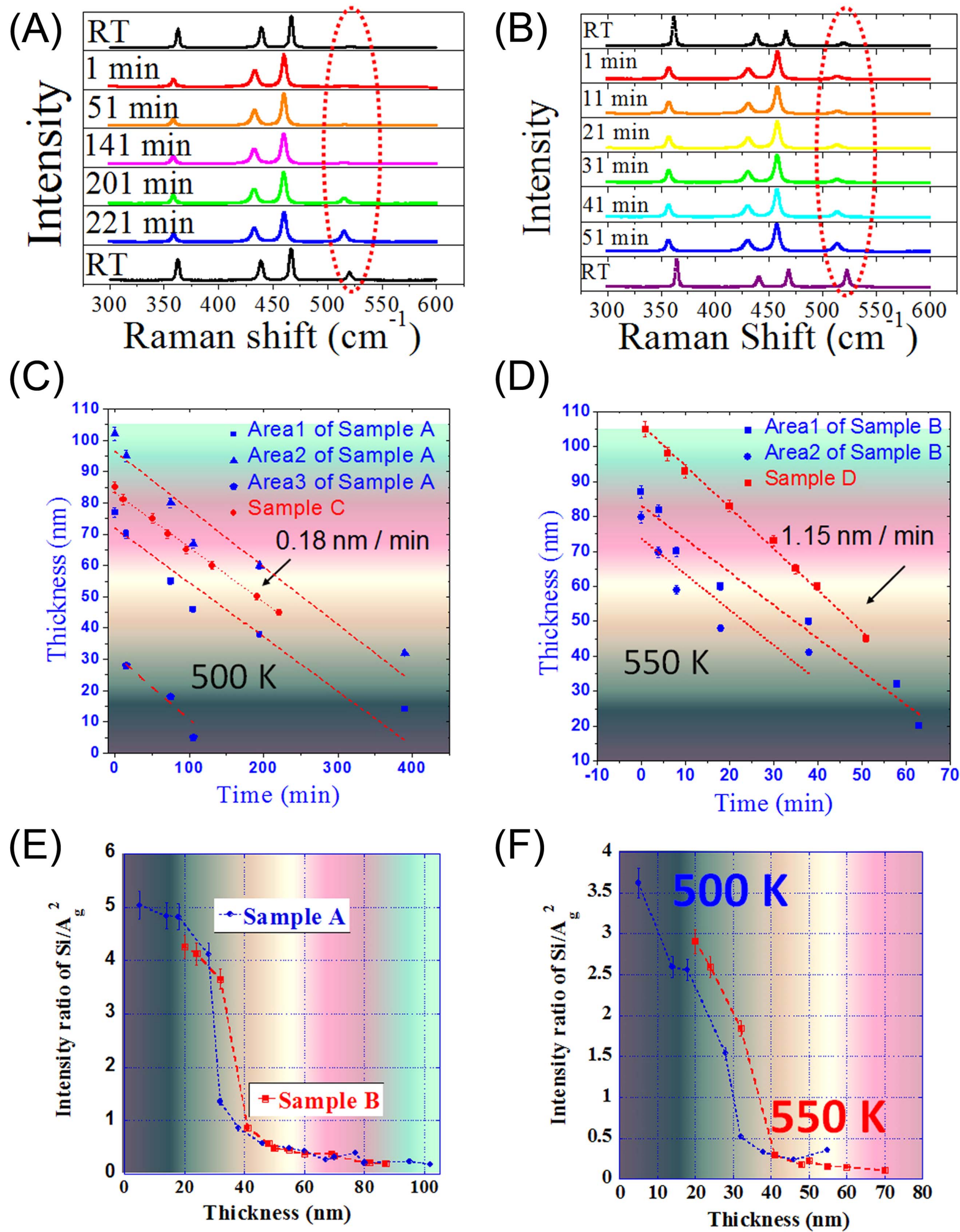

Figure 5. (A) The *in situ* Raman spectra of 'Sample C' collected at 500 K; (B) the *in situ* Raman spectra of 'Sample C' collected at 550 K. (C) The comparison of thinning rates of 'Sample A' ('interrupted heating') and C ('continuous heating') at 500 K; (D) the comparison of thinning rates of 'Sample B' ('interrupted heating') and D ('continuous heating') at 550 K. (E) The room temperature Raman intensity ratios of $\frac{\mathrm{Si}}{\mathrm{A}_g^2}$ as a function of measured thickness; (F) the high temperature Raman intensity ratios of $\frac{\mathrm{Si}}{\mathrm{A}_g^2}$ as a function of measured thickness. To note that, in (E) and (F), the blue line represents 'Sample A' heated at 500 K and red line indicates 'Sample B' heated at 550 K, respectively.

Raman intensity ratios $\frac{I_{\mathrm{Si}}}{I_{\mathrm{A}_g^2}}$ increased with decreasing thickness. On the other hand, as the CO determinations were done at 'Sample A' and 'Sample B', and assuming that there is little thickness change during the ramp up and the cooling down process, and with the known thickness before and after thinning cycle, we plotted the Raman intensity ratios of underlying Si over BP A_g^2 mode ($\frac{I_{\mathrm{Si}}}{I_{\mathrm{A}_g^2}}$) as functions of the thicknesses of 'Sample A' and 'Sample B' measured by AFM at three different measurement temperatures: room temperature (300 K), 500 and 550 K. In figure 5(E), both room temperature profiles of 'Sample A' and 'Sample B' match, and the ($\frac{I_{\mathrm{Si}}}{I_{\mathrm{A}_g^2}}$) ascends with the decreasing thickness; meanwhile; in figure 5(F), *in situ* ($\frac{I_{\mathrm{Si}}}{I_{\mathrm{A}_g^2}}$) curves at the heating temperature of 'Sample A' (500 K) and B (550 K) were given. This ratio has a temperature dependence as the Si and BP Raman peaks have different temperature dependence. With known COs of BP and Si that were

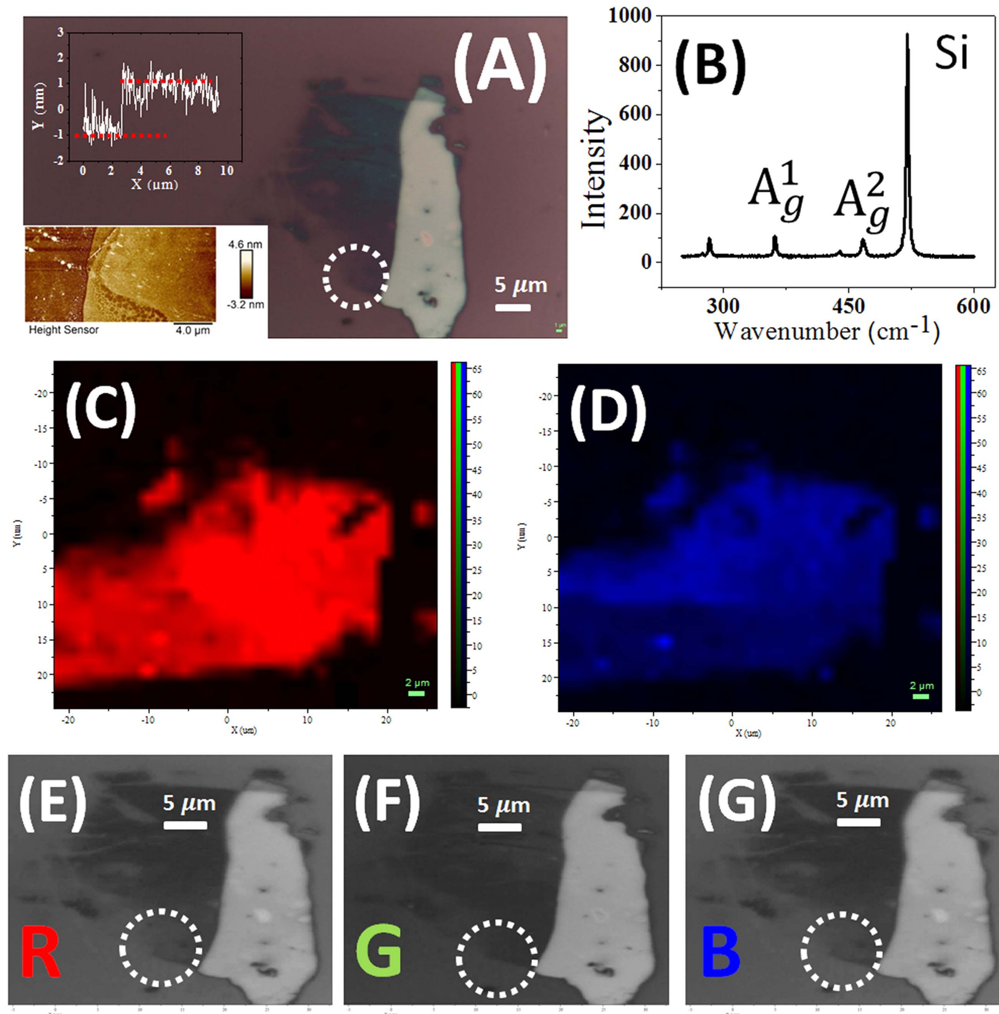

Figure 6. Determination of the thickness and characterization of the crystallinity of 'Sample A'. (A) The optical image of 'Sample A', area 3 was circled; (B) the Raman spectrum of circled area in (A). (C) and (D) The 2D Raman maps of A_g^1 and A_g^2 modes of 'Sample A'; (E)–(G) the red, green and blue channel images of (A).

measured before heating, these Raman intensity ratio profiles could provide the capability of the *in situ* determination of BP thickness at 500 K and 550 K, respectively.

Furthermore, previous studies [33, 34] have reported that, in order to establish the relationship between the layer number N of 2-dimensional materials such as graphene and the Raman intensity ratio $\frac{I_{2DM}}{I_{Si}}$, it is necessary to keep the same CO of Si substrate during the intensity measurement for each sample. Similarly, in this work, as the polarization orientation dependence of both BP and Si Raman peaks has been well-studied, we proposed that, with known CO of Si, the measured Si Raman intensity could be normalized in respect to the maximum Si Raman intensity according to the angle difference, then the relationship between the layer number N of BP and the Raman intensity ratio $(\frac{I_{Si}}{I_{A_g^2}})$ can be used as an effective method in determining and controlling the thickness of BP during heating.

3.3. The thinning limit: preparation of two-layer to four-layer BP

To study the effectiveness of the thermal thinning method in preparing large few-layer crystalline BP, we performed an additional cycle of heating at the processed 'Sample A' shown in figure 4(A). The results were shown in figure 6: in figure 6(A), 'Area 3' was entirely sublimated. In figures 6(B)–(D), the Raman spectrum at the circled position of figure 6(A) and spatial Raman maps of A_g^1 and A_g^2 modes indicate the crystallinity of the BP sample was still retained. In addition, we measured the thickness of the circled area by AFM. The AFM image and the height profile are shown in the inset image and profile incorporated in figure 6(A), which indicate that the thickness of 'Area 1' was reduced to ~2 nm thick (~4 layers).

The optical contrast has been demonstrated to be a useful tool in determining 2D materials below a few nanometers [47, 48], we applied this method in confirming the BP

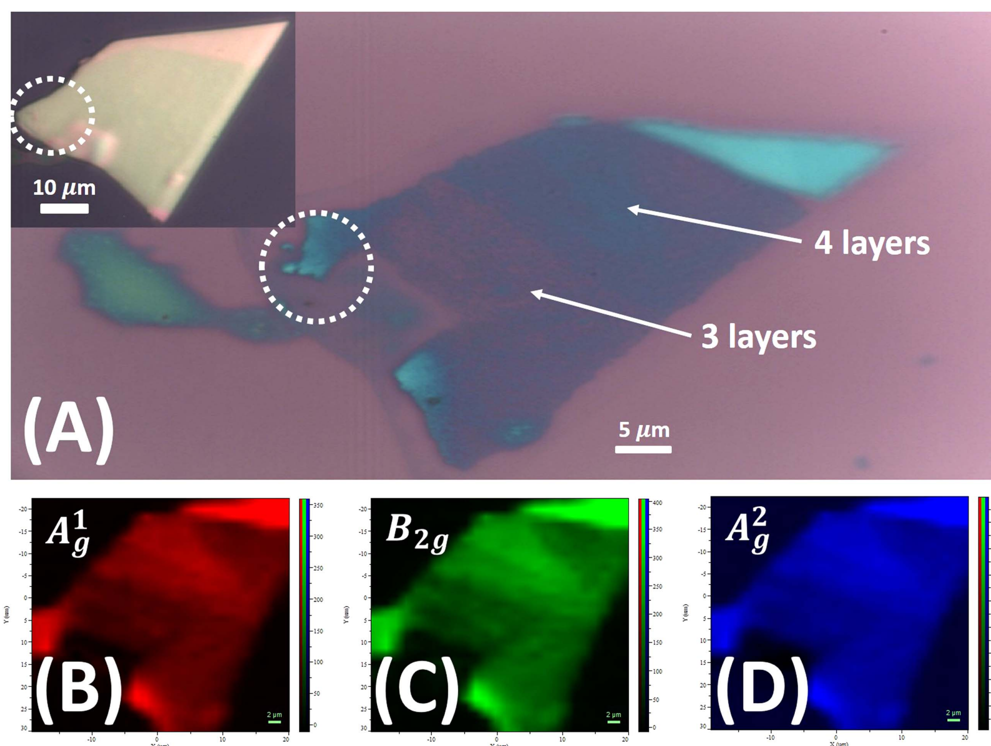

Figure 7. (A) The prepared BP sample with an area over 1000 μm^2, and inset image shows the original sample; (B)–(D) the Raman imaging results of the 3 BP Raman modes: A_g^1, B_{2g} and A_g^2, respectively.

thickness. We splitted figure 6(A) into monochromic red (R), green (G), and blue (B) channel images via Image J [49] shown in figures 6(E) and (F). Here we choose the highest-contrast gray-scale image in the G channel shown in figure 6(F). According to Gomez *et al* [19]'s report, the monolayer BP showed an optical absorbance of 2.8%, while bilayer BP flakes showed an optical absorbance of $5.5 \pm 0.2\%$. In this work, the optical contrast of the area in figure 6(F) showed a mean value of 10.89%, which corresponds to 4-layer BP. Therefore, the thickness from the optical contrast was in agreement with the AFM result.

We prepared multiple large few-layer BP flakes via the thermal thinning method. In figure 7(A), we demonstrated the successful preparation of a thin BP flake with an area over $\sim 1000\,\mu m^2$ by continuously heating a thick bulk BP flake (see the inset image of figure 7(A)) at 573 K under N_2 protection. The entire sample retained its integrity in micron scale as observed by the 2D Raman mapping after the heating process. The optical contrast (shown in figure S6 of supplementary information) results showed the sample in figure 7(A) had two areas with the mean optial contrast values of 7.21% and 10.96%, corresponding to 3-layer and 4-layer BP. In 2D Raman maps of this sample (figures 7(B)–(D)), the BP vibrational modes A_g^1, B_{2g} and A_g^2 showed strong intensities in comparison with the substrate, which indicated the crystallinity of the BP flake.

After that, we prepared another 2 independent few-layer BP flakes (shown in figures S7(A) and (B) of supplementary information): the sample in figure S7(A) had an area of $\sim 250\,\mu m^2$, and the optical contrast showed a mean value of 9.20%, corresponding to 4 layers; the sample in figure S7(B) had two areas. The optical contrast results showed two means values of 6.52% and 7.68%, corresponding to bilayer and 3 layers. In addition, Raman mapping results (see figures S8 and S9 in supplementary information) also indicated good crystallinity of both samples. Overall, our results showed that sublimation is an effective method for thinning large area BP down to bilayers.

3.4. Thermal thinning on other substrates and quality of thermally thinned BP

In addition, via the thermal thinning method, we successfully prepared a large few-layer BP on top of a multiple-layer graphene/Si substrate. Figure 8(B) shows that the BP flake in figure 8(A) is thinned down to few-layers (with an optical contrast of 10.34%, corresponding to 4 layers) after 3 cycles of 'interrupted heating' at 300 °C. Figure 8(C) shows that after each cycle of heating, the Si Raman peak intensity was enhanced which indicated that the thickness of BP decreased. However, the three BP Raman modes at 361.37, 437.9 and 465.44 cm^{-1} still remained. After the second heating cycle, the G band and 2D band at 1599.01 and 2739.82 of graphene were visible in the Raman spectra. In another study by the authors, we successfully prepared large few-layer BP flakes on polyimide substrates [38]. The results indicated that: (1) BP can be also thinned down on graphene/Si and polyimide substrates; (2) this method is promising for controllably preparing BP/graphene and other 2D heterostructures.

After our initial report in January 2016 [50], Robbins *et al* [51] recently used a similar thermal thinning method and

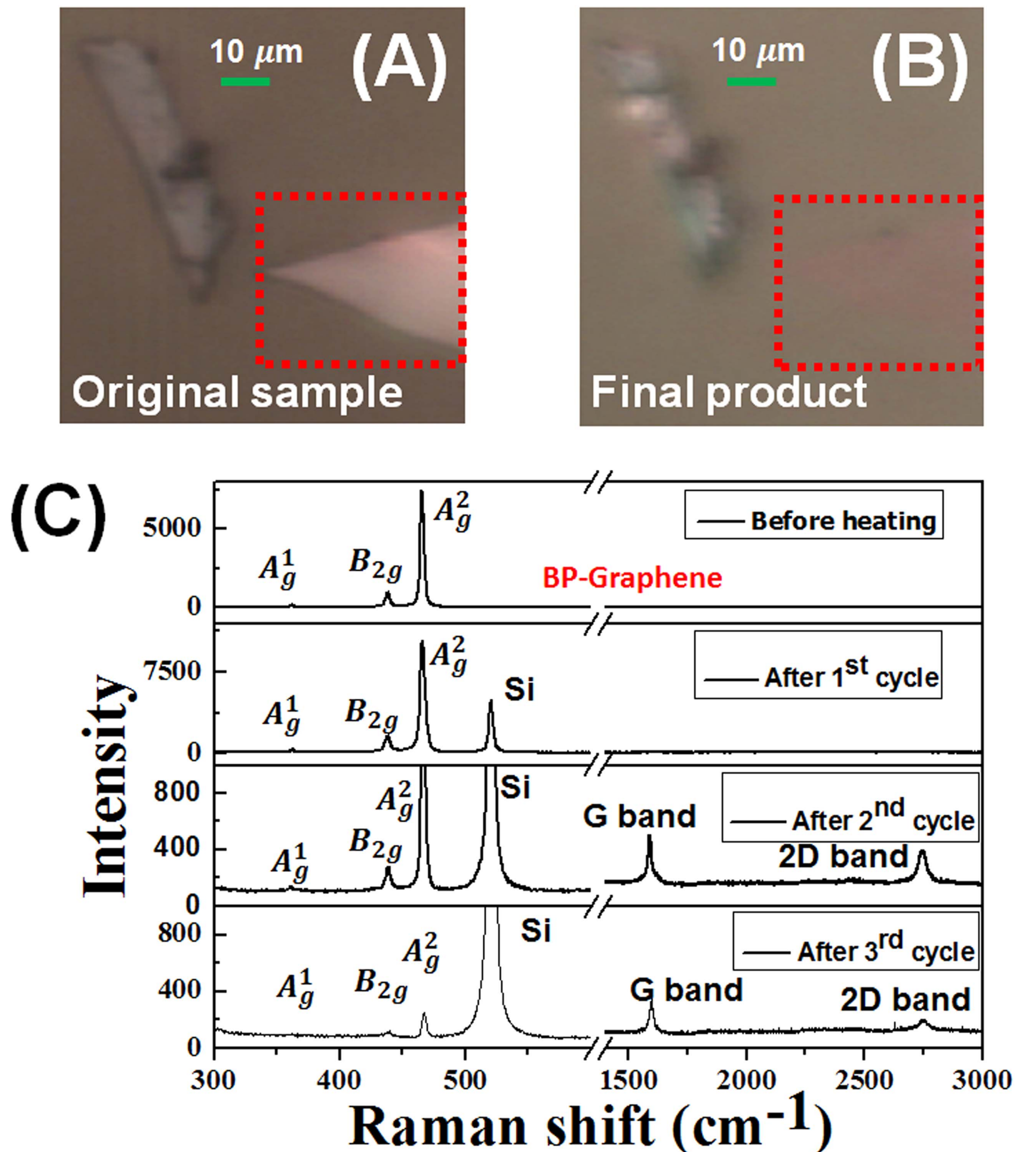

Figure 8. (A) Original BP sample on multiple layer graphene/Si wafer substrate prepared by mechanical exfoliation; (B)–(D) the final BP flake which was thinned down to ~4 layers; (C) the Raman spectra collected before heating and after each cycle of heating.

reported that BP heterostructure MOSFETs were successfully fabricated on thermally thinned BP flakes showing good transistor behaviors. Although their BP flakes were thinned in vacuum instead of in nitrogen as in this work, their work proved the suitableness of thermally thinned BP in device applications.

4. Conclusion

In summary, this work reported on the layer-by-layer sublimation of BP at 500–600 K. The thinning rates for 'continuous heating' were $\sim$0.18 nm min^{-1} and 1.15 nm min^{-1} at 500 and 550 K, respectively. The Raman intensity ratios of $\frac{I_{Si}}{I_{A_g^2}}$ as functions of BP thickness at room temperature, 500 and 550 K were measured, which could be used as an *in situ* and non-contact determination of BP thickness and thickness control during the sublimation thinning process. Large (with areas >200 μm^2) and few-layer (2–4 layers) BP flakes with good integrity, uniformity and crystallinity on Si wafer and graphene/Si substrate were prepared successfully and repeatedly. No micron scale defects were observed. We expect this method also works for deposited BP besides exfoliated BP. The sublimation thinning method is promising in further fabrication of high quality few-layer BP in large scale.

Acknowledgments

The authors acknowledge Dr David Tuschel (Horiba Scientific, Edison, NJ, USA) for discussions on angle-resolved polarized Raman spectroscopy. The authors acknowledge Chris Balicki (4D LABS, Simon Fraser University, Burnaby, BC, Canada) for his assistance in Atomic Force Microscopy and Ms. Zenan Jiang (Electrical Engineering, University of British Columbia, Vancouver, BC, Canada) for supplying the CVD graphene.

Author contributions

WL and GX conceived the experiments. WL conducted more than 90% of the thermal thinning, Raman measurements and analyzed the results. WL prepared the majority of the samples and performed the majority of the AFM measurements. RY and Y Zhao contributed by some AFM and Raman measurements respectively. J Liu and W Zhu contributed by providing initial samples and helpful discussions. WL and GX led the writing of the paper, and all the authors participated in the discussions of results. The project was supervised by GX All authors reviewed the manuscript.

ORCID

Weijun Luo https://orcid.org/0000-0002-6048-5164

References

[1] Ling X, Wang H, Huang S, Xia F and Dresselhaus M S 2015 The renaissance of black phosphorus *Proc. Natl Acad. Sci.* **112** 4523–30
[2] Liang L, Wang J, Lin W, Sumpter B G, Meunier V and Pan M 2014 Electronic bandgap and edge reconstruction in phosphorene materials *Nano Lett.* **14** 6400–6
[3] Takao Y, Asahina H and Morita A 1981 Electronic structure of black phosphorus in tight binding approach *J. Phys. Soc. Japan* **50** 3362–9
[4] Li L, Yu Y, Ye G J, Ge Q, Ou X, Wu H, Feng D, Chen X H and Zhang Y 2014 Black phosphorus field-effect transistors *Nat. Nanotechnol.* **9** 372–7
[5] Kim J S, Jeon P J, Lee J, Choi K, Lee H S, Cho Y, Lee Y T, Hwang D K and Im S 2015 Dual gate black phosphorus field effect transistors on glass for nor logic and organic light emitting diode switching *Nano Lett.* **15** 5778–83
[6] Koenig S P, Doganov R A, Schmidt H, Neto A C and Oezyilmaz B 2014 Electric field effect in ultrathin black phosphorus *Appl. Phys. Lett.* **104** 103106
[7] Das S, Demarteau M and Roelofs A 2014 Ambipolar phosphorene field effect transistor *ACS Nano* **8** 11730–8
[8] Du Y, Liu H, Deng Y and Ye P D 2014 Device perspective for black phosphorus field-effect transistors: contact resistance, ambipolar behavior, and scaling *ACS Nano* **8** 10035–42
[9] Abbas A N, Liu B, Chen L, Ma Y, Cong S, Aroonyadet N, Köpf M, Nilges T and Zhou C 2015 Black phosphorus gas sensors *ACS Nano* **9** 5618–24
[10] Sun L-Q, Li M-J, Sun K, Yu S-H, Wang R-S and Xie H-M 2012 Electrochemical activity of black phosphorus as an anode material for lithium-ion batteries *J. Phys. Chem.* C **116** 14772–9
[11] Qin G, Yan Q-B, Qin Z, Yue S-Y, Cui H-J, Zheng Q-R and Su G 2014 Hinge-like structure induced unusual properties of black phosphorus and new strategies to improve the thermoelectric performance *Sci. Rep.* **4** 6496
[12] Choi S J, Kim B-K, Lee T-H, Kim Y H, Li Z, Pop E, Kim J-J, Song J H and Bae M-H 2016 Electrical And thermoelectric transport by variable range hopping in thin black phosphorus devices *Nano Lett.* **16** 3969–75 arXiv:1404.5171
[13] Low T, Engel M, Steiner M and Avouris P 2014 Origin of photoresponse in black phosphorus phototransistors *Phys. Rev.* B **90** 081408
[14] Wang Y, Huang G, Mu H, Lin S, Chen J, Xiao S, Bao Q and He J 2015 Ultrafast recovery time and broadband saturable absorption properties of black phosphorus suspension *Appl. Phys. Lett.* **107** 091905
[15] Castellanos-Gomez A 2015 Black phosphorus: narrow gap, wide applications *J. Phys. Chem. Lett.* **6** 4280–91
[16] Ryder C R, Wood J D, Wells S A, Yang Y, Jariwala D, Marks T J, Schatz G C and Hersam M C 2016 Covalent functionalization and passivation of exfoliated black phosphorus via aryl diazonium chemistry *Nat. Chem.* **8** 597–602
[17] Wood J D, Wells S A, Jariwala D, Chen K-S, Cho E, Sangwan V K, Liu X, Lauhon L J, Marks T J and Hersam M C 2014 Effective passivation of exfoliated black phosphorus transistors against ambient degradation *Nano Lett.* **14** 6964–70
[18] Luo W, Zemlyanov D Y, Milligan C A, Du Y, Yang L, Wu Y and Peide D Y 2016 Surface chemistry of black phosphorus under a controlled oxidative environment *Nanotechnology* **27** 434002
[19] Castellanos-Gomez A *et al* 2014 Isolation and characterization of few-layer black phosphorus *2D Mater.* **1** 025001
[20] Liu X, Chen K-S, Wells S A, Balla I, Zhu J, Wood J D and Hersam M C 2016 Scanning probe nanopatterning and layer-by-layer thinning of black phosphorus *Adv. Mater.* **29** 1604121
[21] Brent J R, Savjani N, Lewis E A, Haigh S J, Lewis D J and O'Brien P 2014 Production of few-layer phosphorene by liquid exfoliation of black phosphorus *Chem. Commun.* **50** 13338–41
[22] Hanlon D *et al* 2015 Liquid exfoliation of solvent-stabilized few-layer black phosphorus for applications beyond electronics *Nat. Commun.* **6** 8563
[23] Seo S, Lee H U, Lee S C, Kim Y, Kim H, Bang J, Won J, Kim Y, Park B and Lee J 2016 Triangular black phosphorus atomic layers by liquid exfoliation *Sci. Rep.* **6** 23736
[24] Lu W, Nan H, Hong J, Chen Y, Zhu C, Liang Z, Ma X, Ni Z, Jin C and Zhang Z 2014 Plasma-assisted fabrication of monolayer phosphorene and its Raman characterization *Nano Res.* **7** 853–9
[25] Lee G, Lee J-Y, Lee G-H and Kim J 2016 Tuning the thickness of black phosphorus via ion bombardment-free plasma etching for device performance improvement *J. Mater. Chem.* C **4** 6234–9
[26] Pei J, Gai X, Yang J, Wang X, Yu Z, Choi D-Y, Luther-Davies B and Lu Y 2016 Producing air-stable monolayers of phosphorene and their defect engineering *Nat. Commun.* **7** 10450
[27] Smith J B, Hagaman D and Ji H-F 2016 Growth of 2d black phosphorus film from chemical vapor deposition *Nanotechnology* **27** 215602
[28] Yang Z, Hao J, Yuan S, Lin S, Yau H M, Dai J and Lau S P 2015 Field-effect transistors based on amorphous black phosphorus ultrathin films by pulsed laser deposition *Adv. Mater.* **27** 3748–54
[29] Huang Y-K, Cain J D, Peng L, Hao S, Chasapis T, Kanatzidis M G, Wolverton C, Grayson M and Dravid V P 2014 Evaporative thinning: a facile synthesis method for high quality ultrathin layers of 2d crystals *ACS Nano* **8** 10851–7
[30] Lu W, Zhang Y, Zhu Z, Lai J, Zhao C, Liu X, Liu J and Sun D 2016 Thin tungsten telluride layer preparation by thermal annealing *Nanotechnology* **27** 414006
[31] Liu X, Wood J D, Chen K-S, Cho E and Hersam M C 2015 *In situ* thermal decomposition of exfoliated two-dimensional black phosphorus *J. Phys. Chem. Lett.* **6** 773–8
[32] Fortin-Descheenes M, Levesque P L, Martel R and Moutanabbir O 2016 Dynamics and mechanisms of

exfoliated black phosphorus sublimation *J. Phys. Chem. Lett.* **7** 1667–74
[33] Li X-L, Han W-P, Wu J-B, Qiao X-F, Zhang J and Tan P-H 2017 Layer-number dependent optical properties of 2d materials and their application for thickness determination *Adv. Funct. Mater.* **27** 1604468
[34] Li X-L, Qiao X-F, Han W-P, Lu Y, Tan Q-H, Liu X-L and Tan P-H 2015 Layer number identification of intrinsic and defective multilayered graphenes up to 100 layers by the Raman mode intensity from substrates *Nanoscale* **7** 8135–41
[35] Lin D Y T 2013 Integrating graphene and nanofibers with silicon to form Schottky junction solar cells *PhD Thesis* University of British Columbia (https://doi.org/10.14288/1.0073579)
[36] Kim J, Lee J-U, Lee J, Park H J, Lee Z, Lee C and Cheong H 2015 Anomalous polarization dependence of Raman scattering and crystallographic orientation of black phosphorus *Nanoscale* **7** 18708–15
[37] Ling X *et al* 2016 Anisotropic electron–photon and electron–phonon interactions in black phosphorus *Nano Lett.* **16** 2260–7
[38] Luo W, Song Q, Zhou G, Tuschel D and Xia G 2016 Study of black phosphorus using angle-resolved polarized Raman spectroscopy with 442 nm excitation arXiv:1610.03382
[39] Wu J, Mao N, Xie L, Xu H and Zhang J 2015 Identifying the crystalline orientation of black phosphorus using angle-resolved polarized Raman spectroscopy *Angew. Chem.* **127** 2396–9
[40] Su L and Zhang Y 2015 Temperature coefficients of phonon frequencies and thermal conductivity in thin black phosphorus layers *Appl. Phys. Lett.* **107** 071905
[41] Favron A, Gaufrès E, Fossard F, Phaneuf-L'Heureux A-L, Tang N Y, Lévesque P L, Loiseau A, Leonelli R, Francoeur S and Martel R 2015 Photooxidation and quantum confinement effects in exfoliated black phosphorus *Nat. Mater.* **14** 826–32
[42] Wang Y, Yang B, Wan B, Xi X, Zeng Z, Liu E, Wu G, Liu Z and Wang W 2016 Degradation of black phosphorus: a real-time 31 p nmr study *2D Mater.* **3** 035025
[43] Li Q, Chen J, Feng Z, Feng L, Yao D and Wang S 2016 The role of air adsorption in inverted ultrathin black phosphorus field-effect transistors *Nanoscale Res. Lett.* **11** 521
[44] Tuschel D 2012 Raman crystallography in theory and in practice *Spectroscopy* **27** 22–7 http://www.spectroscopyonline.com/raman-crystallography
[45] Yoo W S, Harima H and Yoshimoto M 2015 Polarized Raman signals from Si wafers: dependence of in-plane incident orientation of probing light *ECS J. Solid State Sci. Technol.* **4** P356–63
[46] Tran V, Soklaski R, Liang Y and Yang L 2014 Layer-controlled band gap and anisotropic excitons in few-layer black phosphorus *Phys. Rev.* B **89** 235319
[47] Li H, Lu G, Yin Z, He Q, Li H, Zhang Q and Zhang H 2012 Optical identification of single-and few-layer MoS_2 sheets *Small* **8** 682–6
[48] Li H, Wu J, Huang X, Lu G, Yang J, Lu X, Xiong Q and Zhang H 2013 Rapid and reliable thickness identification of two-dimensional nanosheets using optical microscopy *ACS Nano* **7** 10344–53
[49] Schneider C A, Rasband W S and Eliceiri K W 2012 Nih image to imagej: 25 years of image analysis *Nat. Methods* **9** 671–5
[50] Luo W, Yang R, Liu J, Zhu W and Xia G 2016 Thermal sublimation: a scalable and controllable thinning method for the fabrication of few-layer black phosphorus arXiv:1601.04103
[51] Robbins M C, Namgung S, Oh S-H and Koester S J 2017 Cyclical thinning of black phosphorus with high spatial resolution for heterostructure devices *ACS Appl. Mater. Interfaces* **9** 12654–62